ap

Asian Journal of Physics

Vol. 26, No 1 (2017) 01-07

Available on: www.asianjournalofphysics.in

Spectroscopy of $^{176}Lu^{+}$

Samuel Wang, Rattakorn Kaewuam, Arpan Roy, K J Arnold and M D Barrett

Centre for Quantum Technologies and Department of Physics National University of Singapore, 3 Science Drive 2, 117543 Singapore

We report spectroscopy of the low-lying 5d6s $^3D_1$, 5d6s $^3D_2$, and 6s6p $^3P_1$ levels of $^{176}Lu^{+}$ relative to the $6s^2\ ^1S_0$ ground state. The hyperfine structure for each level, the allowed electric dipole transitions, and clock transitions between the *S* and *D* states are all determined to the ~MHz level of accuracy. These measurements provide a useful starting point for establishing optical clock operation with this isotope.

Keywords: Optical clocks, Spectroscopy.

1 Introduction

Singly ionized lutetium has recently been proposed as a promising optical clock candidate [1,2]. The $^1S_0 - {}^3D_1$ clock transition is a highly forbidden magnetic dipole transition, which has a number of properties suitable for clock operation. Large hyperfine and fine structure splittings together with the technique of hyperfine averaging promises to realize an effective $J = 0$ to $J' = 0$ transition with low sensitivity to magnetic fields [1]. A narrow electric dipole transition provides the possibility of a low Doppler cooling limit and suitable detection. The differential static scalar polarizability is expected to be sufficiently small for practical room temperature operation and potentially negative which would allow micro-motion shifts to be eliminated [3,4]. A negative value in particular is critical for realizing a recent proposal for clock operation with large ion crystals [2]. Clock operation for the more abundant $^{175}Lu^{+}$ isotope has been demonstrated [5], but $^{176}Lu^{+}$, with a nuclear spin $I = 7$, is more desirable. The integer nuclear spin allows the use of $m = 0$ clock states which are inherently less sensitive to magnetic fields

Spectroscopy of $^{176}Lu^{+}$ is more difficult owing to its relatively low abundance of ~2.5% and limited data is available in the literature. The hyperfine splitting of the 5d6s $^3D_1$ and 6s6p $^3P_1$ levels with accuracies of 10-20 MHz have been reported but optical frequencies are much less accurately known [6,7]. Here we perform optical spectroscopy on a single trapped $^{176}Lu^{+}$ that is sympathetically cooled by $^{138}Ba^{+}$. Optical frequencies are referenced to an optical comb, and accuracy at the MHz level is achieved.

2 Experimental Apparatus.

The experiments are performed in a four-rod linear Paul trap with axial end caps, similar to the one described in [5]. The trap consists of four electro-polished beryllium copper rods of 0.45 mm diameter arranged on a square of sides 1.2 mm in length. A 16.8 MHz rf potential is applied to two of the opposing diagonal rods via a helical quarter-wave resonator. A -0.1 V DC bias is applied to other two rods. Axial confinement is provided by 8 volts DC applied to the end caps with a separation of 2 mm. In this configuration, the measured trap frequencies are $(\omega_x,\omega_x,\omega_x) = 2\pi \times (740,766,188)$ kHz. These frequencies are measured using a single $^{138}Ba^{+}$ion, which is present throughout to provide sympathetic cooling.

Corresponding author :
e-mail: phybmd@nus.edu.sg (M D Barrett)

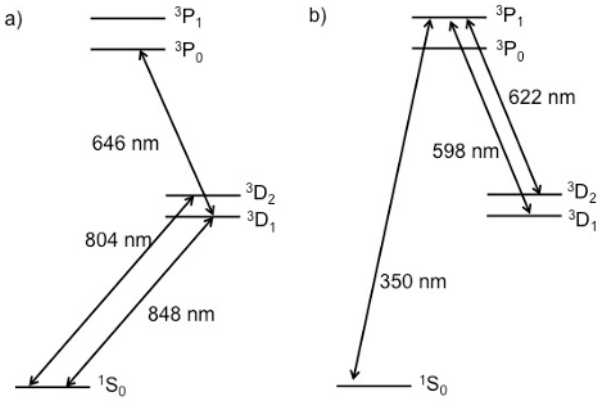

Fig 1. Level structure of Lu^+: (a) the two clock transitions at 804-nm and 848-nm and the detection transition at 646-nm and (b) Optical pumping transitions at 350-nm, 598-nm and 622-nm.

The relevant level structure for lutetium is given in Fig 1, which shows the transitions used in this work. There are two clock transitions: a magnetic dipole transition, $^1S_0 - {}^3D_1$, at 848-nm,and an electric quadrupole transition, $^1S_0 - {}^3D_2$, at 804 nm. Diode lasers stabilized to high finesse reference cavities drive these transitions and propagate orthogonally to a magnetic field. All other transitions are dipole transitions and their respective laser fields are linearly polarized perpendicular to the magnetic field.

The 350-nm laser addressing the $^1S_0 - {}^3P_1$ transition is a frequency-doubled diode with the fundamental locked to a transfer cavity. The transfer cavity is referenced by a diode laser at 852-nm which is locked to a cesium vapor cell. The 598-nm laser is also a frequency doubled diode laser and it is directly stabilized to a wavemeter with specified ~10MHz accuracy. The 646-nm laser addressing the $^3D_1 - {}^3P_0$ transition is a diode laser stabilized to a transfer cavity referenced as for the 350-nm laser system.

The 622-nm laser addressing the $^3D_2 - {}^3P_1$ transition is also a diode laser. A wideband electro-optic modulator (EOM) is driven with multiple sidebands to address all 5 levels of $^3D_2$. This requires *a priori* information on the hyperfine structure of the $^3D_2$ and $^3P_1$ levels. Hyperfine structure for $^3P_1$ is reported in [6]. For $^3D_2$ an estimate was made using the values reported in [7] for $^{175}Lu^+$ and rescaling estimated hyperfine A and B coefficients with known nuclear dipole and quadrupole moments [8].

3 Experiments

3.1 Detection

Detection is achieved via scattering on the $^3D_1 - {}^3P_0$ transition. To address the three separate hyperfine levels, a wideband EOM generates sidebands of approximately 10.5 GHz to address the F = 6, and 8 hyperfine levels. A separate carrier beam is shifted by a double passed acousto-optic modulator (AOM) to address the remaining F = 7 level. Both beams are then combined into a single fiber. Settings of the EOM and AOM were initially chosen to match the hyperfine structure of $^3D_1$ reported in [6].

In order to obtain fluorescence, the ion must first be optically pumped into $^3D_1$ with the 350- and 622-nm lasers. Successful detection thus requires all three lasers to be correctly set. Fortunately, as discussed in [4], quenching of the fluoresce rate for the $^3D_1 - {}^3P_0$ transition occurs through hyperfine induced mixing between fine-structure levels. This results in decay to either $^1S_0$ or $^3D_2$ from the upper $^3P_0$ state. This rate is rather slow and fluoresce can be observed on the one second timescale before decay from the detection channel occurs. Hence the 350- and 622-nm lasers can be fairly crudely set in order to optimize the offset frequency of the 646-nm laser.

Under continuous excitation from the 350-, 622-, and 646-nm lasers, the 646-nm fluorescence rate intermittently falls to a low value signaling decay to either $^1S_0$ or $^3D_2$. The length of time the signal remains low is determined by the pumping rates provided by the 350-, and 622-nm lasers. Hence the frequencies of these lasers can be adjusted to minimize the pumping times out of the dark state. However, as the 622-nm laser involved multiple sidebands, we can only optimize the pumping time as a function of the carrier frequency. Further refinement of the 622-nm laser requires more exact determination of the $^3P_1$ and $^3D_2$ hyperfine structures as outlined in Sect. 3.2, and 3.4.

We note that an improvement in the positioning of the 622-nm sidebands can be obtained using the 598-nm laser. When both the 598-nm and 646-nm lasers are on, the ion is rapidly pumped into a dark state if the 598-nm laser is tuned to one of six transitions between $^3D_1$ and $^3P_1$. Since the 598-nm laser could not be referenced to the comb, this approach is limited by the 10 MHz accuracy of the wavemeter used to determine the 598-nm frequency. This is sufficient to provide optical pumping times of a few microseconds, but a more accurate approach is described in Sect. 3.4.

3.2 $^3P_1$ structure

To provide a more accurate measurement of the hyperfine structure of $^3P_1$ and a measurement of the optical frequency of the 350-nm laser, we optimize pumping times out of $^1S_0$. The ion is first prepared in $^1S_0$ by optically pumping with the 598-, 622- and 646-nm lasers. We then optically pump for 40us with the 350-nm laser before measuring the population in the $^3D_1$ state. From the known branching ratios for decays out of $^3P_1$, at most ~30% of the population returns to $^3D_1$ [4]. Hence the 350-nm laser is attenuated to avoid complete pumping out of $^1S_0$ while still providing a sufficient signal-to-noise for the bright state measurement. Note that these measurements were carried out at a magnetic field of 0.48 mT.

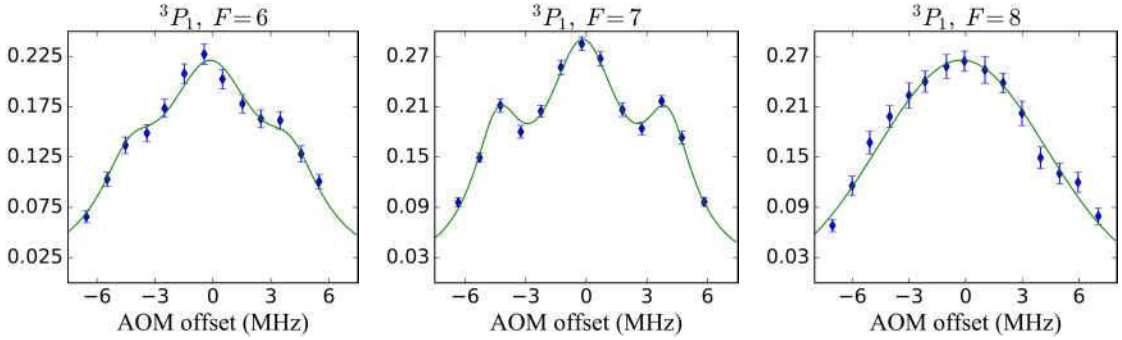

Fig 2. Optical pumping out of $^3P_1$. For each upper F state, we measure the population pumped into $^3D_1$ in 40 us. Fits include a sideband at the 16.8 MHz RF drive of the trap. Frequencies are relative to a set point of an AOM, which is double passed before the doubling cavity.

In Fig 2, we show the measured populations as a function of the drive frequency of an AOM relative to a fixed set point. The AOM is in a double pass configuration and shifts the frequency of the 700nm laser. Thus the frequency offset of the 350nm laser is four times that of the AOM frequency. The center point of each plot is determined by a least square fit. For F = 6, and 7 this fit includes a micromotion sideband corresponding to the 16.8 MHz RF trap drive which is clearly present in the data. The frequency of the 350-nm laser corresponding to the center points of each figure were determined by referencing the 700-nm laser against a frequency comb and are given by

f_6 = 854 473 362.8 (1.4) MHz

f_7 = 854500432.9 (1.2) MHz

f_8 = 854526226.8 (1.5) MHz

where the subscript denotes the F level of $^3P_1$. The quoted errors account for drifts of the oscillators used to drive the AOM's controlling the 350-nm laser over the time scale of the experiment, which was determined by monitoring the comb beat signal over several hours. From these values we then obtain the hyperfine splittings

$f_7 - f_6 = 27\,070.1\ (1.9)$ MHz

$f_8 - f_7 = 25\,793.9\ (2.0)$ MHz

These differ by about +75 MHz and +20 MHz, respectively from previous measurements which were given to 10^{-3} cm^{-1} ~ 30 MHz precision [6].

3.3 $^3D_1$ structure

The determination of the $^3D_1$ hyperfine structure makes use of quantum jumps. When the 848-nm clock laser and the 646-nm laser are both on, the ion makes intermittent jumps to the upper state, which brightly fluoresces. The presence of the 646-nm laser effectively broadens the transitions to the level of a few MHz but the extremely small line-width of the clock transition results in long timescales between quantum jumps. Experimentally we slowly scan the 848-nm laser back and forth over a given range of frequencies and record the frequencies at which quantum jumps occur. This gives histogramsas shown in Fig 3. The 848-nm laser is locked to a reference cavity with an offset set by a wide band EOM. The reference point in each histogram is an arbitrarily chosen point at which the optical frequency of the 848-nm laser is characterized by a frequency comb.

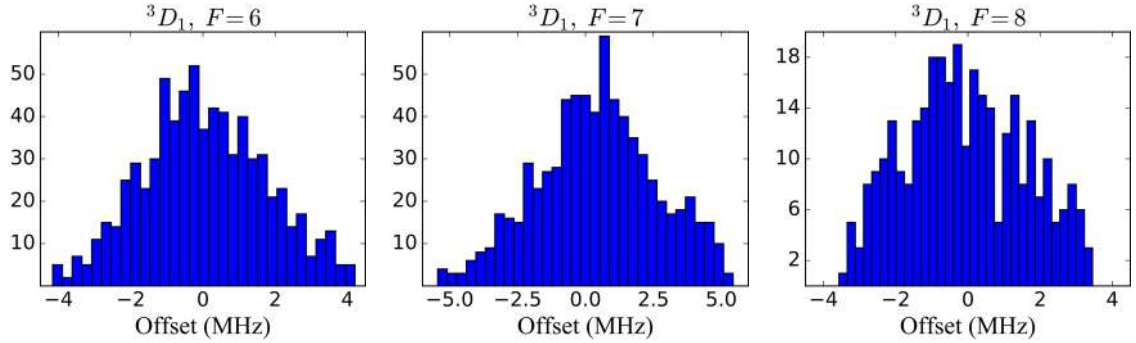

Fig 3. Quantum jumps from $^1S_0$ to $^3D_1$ as a function of offset from a reference point measured against an optical comb.

We take the mean of the distributions as an estimate for the clock transition and the associated optical frequencies are determined by referencing to an optical comb. Drift of the reference cavity over the duration of the data collection is less than the statistical error in determining the mean (~ 0.1 MHz). However, we conservatively add an error bar of 1 MHz to account for any possible AC stark shifts from the 646-nm excitation laser. The clock frequencies are thus

$f_6 = 353649817.8\ (1.1)$ MHz

$f_7 = 353638527.7\ (1.1)$ MHz

$f_8 = 353628036.7\ (1.1)$ MHz

giving hyperfine splittings

$f_6 - f_7 = 11\,290.1\ (1.6)$ MHz

$f_7 - f_8 = 10\,491.0\ (1.6)$ MHz.

Compared to the values given in [6], there is a difference of +18 MHz and +30 MHz consistent with the precision given. Compared to the values given in [9], there is a difference of +15 MHz and –7 MHz. This is significant at the 10^{-4} cm^{-1} ~ 3 MHz precision given in that work.

3.4 $^3D_2$ structure

The time scale for optical pumping out of $^3D_2$ depends on five frequency settings of the 622-nm laser. Thus optimization of pumping times is impractical. Instead we use a quantum jump approach as for the $^3D_1$ case. When the 804-nm clock laser is tuned near to an allowed transition it is promoted to $^3D_2$ and the 622-nm laser optically pumps it back to $^1S_0$ or $^3D_1$. Ultimately it is pumped back to the $^3D_1$ bright state. Hence the presence of the 804-nm clock laser and the 622-nm laser provides intermittent jumps between the $^1S_0$ and $^3D_1$ states as in the previous section

As discussed in the previous section, we scan the clock laser back and forth over a given range of frequencies and record the frequencies at which quantum jumps occur. We insure that the intensity of the 804-nm laser is sufficiently low that returns to the dark state can be clearly identified. The laser is locked to a reference cavity similar to the 848-nm laser and histograms for each of the 5 transitions are given in Fig 4. As in the $^3D_1$ case, the reference point in each histogram is an arbitrarily chosen point at which the optical frequency of the 804-nm laser is characterized by a frequency comb. The reference cavity for the 804-nm has significantly larger drifts relative to the 848-nm cavity. Referencing the laser to a frequency comb periodically throughout the data collection compensated this drift. We also note that, for excitation to $F = 5$, the polarization of the laser was perpendicular to the B-field so as to allow $\Delta m = \pm 2$ transitions to be driven.

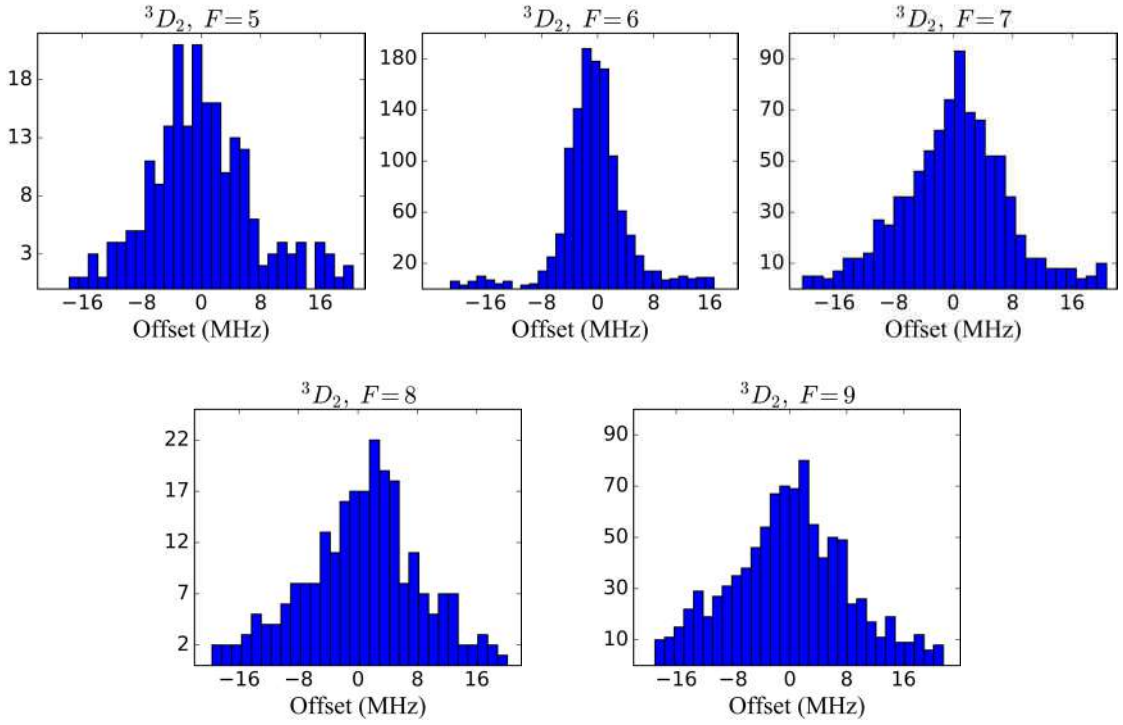

Fig 4. Quantum jumps from $^1S_0$ to $^3D_2$ as a function of 804-nm laser frequency. Laser is locked to a reference cavity and the frequency periodically monitored by an optical comb. The offset is relative to a point at which the optical frequency was measured against a comb.

We take the mean frequency of each histogram to determine the transition frequency. As in the previous section, we add a 1 MHz to the statistical error of the mean to account for any potential stark shifts from the 622-nm laser. The optical frequencies for each transition are then given by

f_9 = 372 817 792.7 (1.3) MHz

f_8 = 372 804 578.0 (1.5) MHz

f_7 = 372 793 515.9 (1.3) MHz

f_6 = 372 784 362.1 (1.2) MHz

f_5 = 372 776 906.0 (1.5) MHz

These then give hyperfine splittings of

$f_9 - f_8$ = 13 214.7 (2.0) MHz

$f_8 - f_7$ = 11 062.1 (2.0) MHz

$f_7 - f_6$ = 9 153.7 (1.8) MHz

$f_6 - f_5$ = 7 456.1 (2.0) MHz

To first order, the hyperfine structure of $^3D_2$ is characterized by four hyperfine constants A, B, C, and D. These coefficients can be determined from the measured hyperfine splitting's provided additional second-order corrections are known. The most significant corrections are the dipole-dipole and dipole-quadrupole interactions, characterized by η and ζ, respectively, which provide mixing with neighbouring fine-structure levels. As noted in [10], the D coefficient is independent of these corrections and can be expressed in terms of the hyperfine splitting's alone. In terms of the optical frequencies, this coefficient is given by

$$D = \frac{11}{214200}\left(204 f_5 - 663 f_6 + 810 f_7 - 442 f_8 + 91 f_9\right)$$

From the measured values of f_k we obtain a value of D = 13 (78) kHz. Thus within the measurement accuracy, the value is consistent with zero.

Measurement accuracy here is limited by resolution of the 804-nm clock transitions. Preparing the ion in a well defined state and driving the clock transition directly would improve the resolution by many orders of magnitude. It is worth noting that, in the expression for the D coefficient, the coefficients of f_k sum to zero. This means that systematic shifts in the determination of the D coefficient largely cancel. For example, consider the possibility of driving $^1S_0$, $m = -1$ to $^3D_2$, $m = 0$ for each F state. The linear Zeeman shift from the ground state cancels leaving only the quadratic shifts from the upper states. These are also suppressed and, from the measurements here, we estimate a magnetic field dependence of ~170 Hz/mT^2. Assuming the transitions are driven with equal intensities, AC stark shifts arising from the probe beam are also suppressed. Contributions from the scalar polarizability cancel completely leaving a shift of $\sim 1.5 \times 10^{-3}\, \alpha_2 \langle E^2 \rangle$ where α_2 is the tensor polarizability. Contributions from the quadrupole moment are similarly suppressed. Hence clock measurements should easily provide an assessment of systematic shifts well below the Hertz level. At this level, second order quadrupole-quadrupole corrections, which are not included in the above expression for D, would likely be significant.

4 Conclusion

To summarize, we have performed spectroscopic measurements of the $^1S_0$ - to -$^3P_1$, $^1S_0$ - to -$^3D_1$, and $^1S_0$ - to - $^3D_2$ transitions in $^{176}Lu^+$. These measurements characterize most of the optical transitions and hyperfine structures relevant to clock operation with this ion. In particular they provide a narrow search window for the clock transitions. The next step is to establish state preparation by optically pumping to the $|7,0\rangle$ state of $^3D_1$, which will enable direct and efficient driving of the 848-nm clock transition.

Acknowledgements

This research is supported by the National Research Foundation, Prime Ministers Office, Singapore and the Ministry of Education, Singapore under the Research Centres of Excellence programme. It is also supported A*STAR SERC 2015 Public Sector Research Funding (PSF) Grant (SERC Project No: 1521200080).

Bibliography

1. Barrett M D, Developing a field independent frequency reference, *New J Phys*, 17(2015)053024; doi.org/10.1088/1367-2630/17/5/053024
2. Arnold Kyle, Hajiyev Elnur, Paez Eduardo, Lee Chern Hui, Barrett M D, Bollinger John, Prospects for atomic clocks based on large ion crystals, *Phys Rev A*, 92(2015)032108; doi.org/10.1103/PhysRevA.92.032108
3. Kozlov A, Dzuba V, Flambaum V V, Optical atomic clocks with suppressed blackbody-radiation shift, *Phys Rev A*, 90(2014)042505; doi.org/10.1103/PhysRevA.90.042505
4. Paez Eduardo, Arnold K J, Hajiyev Elnur, Porsev S G, Dzuba V A, Safronova U I, Safronova M S, Barrett M D, Atomic properties of Lu^{+}, *Phys Rev A*, 93(2016)042112; doi.org/10.1103/PhysRevA.93.042112
5. Arnold K J, Kaewuam R, Roy A, Paez E, Wang S, Barrett M D, Observation of the $^{1}S_0$ to $^{3}D_1$ clock transition in $^{175}Lu^{+}$, *Phys Rev A*, 94(2016)052512; doi:10.1103/PhysRevA.94.052512
6. Schuler Von H, Gollow H, Uber das mechanische und magnetische Moment und uber das Quadrupolmoment des seltenen 176Cp-Kernes, *Zeitschrift fur Physik*, 113(1939)1-9,
7. Schuler Von H, Schmidt Th, Uber die Abweichung des Cassiopeiumatomkerns von der Kugelsymmetrie, *Zeitschrift fur Physik*, 95(1935)265-272.
8. Georg U, Borchers W, Keim M, Klein A, Lievens P, Neugart R, Neuroth M, Rao Pushpa M, Schulz C, and the ISOLDE Collaboration, Laser spectroscopy investigation of the nuclear moments and radii of lutetium isotopes, *Euro Phys J: A*, 3(1998)225-235.
9. Blaise Jean, Bauche Jacques, Gerstenkorn Simon, Tomkins Frank S, Determination spectroscopique du spin de ^{176}Lu et des moments nucleaires magntique et quadrupolaire de ^{175}Lu et ^{176}Lu, *J Phys Radium*, 22(1961)417-427,
10. Beloy K, Derevianko A, Johnson W R, Hyperfine structure of the metastable $^{3}P_2$ state of alkaline-earth-metal atoms as an accurate probe of nuclear magnetic octupole moments, *Phys Rev A*, 77(2008)012512; doi:10.1103/PhysRevA.77.012512

[*Received*: 8. 12. 2016; *accepted*:1.1.2017]